DOI 10.1007/s11141-022-10182-3
Radiophysics and Quantum Electronics, Vol. 64, No. 12, May, 2022
(Russian Original Vol. 64, No. 12, December, 2021)

MICROWAVE AND LIDAR MEASUREMENTS OF OZONE AND TEMPERATURE VARIATIONS DURING STRATOSPHERIC WARMINGS OF 2012–2015

Yu. Yu. Kulikov,[1] * V. N. Marichev,[2] V. M. Demkin,[3] A. A. Krasil'nikov,[1] V. G. Ryskin,[1] G. G. Matvienko,[2] and D. A. Bochkovsky [2]

UDC 551.510.534+550.388.8

We present the results of joint observations of ozone and temperature in the middle atmosphere above Tomsk in December–January 2012–2013 and in December–February 2014–2015 during stratospheric warmings. The results of simultaneous microwave observations of ozone in Peterhof (60° N, 30° E) and Tomsk (56° N, 85° E) in the winter of 2013–2014 are also given. Ground-based microwave radiometry and laser diagnostics were used in the observations. Microwave radiometry and lidar technology allow us to study ozone and temperature variations during large-scale wave disturbances in the middle atmosphere such as stratospheric warming.

1. INTRODUCTION

Stratospheric warmings mostly disturb the dynamics and thermal structure of the winter middle atmosphere in the Northern hemisphere. The development of stratospheric warmings is related to the vertical propagation of planetary waves, which dissipate (lose energy) first in the mesosphere and then gradually in the stratosphere. These waves interact with the western winter circulation of the atmosphere and modify its temperature profile from the upper troposphere to the mesosphere [1].

Strong warmings (of the major type) destroy the winter circulation through the displacement or splitting of the polar vortex, build-up of the eastern circulation, and change of the latitudinal temperature gradient. Significant differences between vortex displacement and vortex splitting events in terms of the dynamics nature, transport, and evolution of the chemical composition of the stratosphere and the vertical structure of the polar vortex take place [2]. Weak warmings (of the minor type) are less intense and cause a change in the middle zonal circulation. Both orbital and ground-based microwave remote sensing tools are widely used to study the middle atmosphere [3, 4]. To interpret the results of these measurements, it is necessary to employ data on the temperature vs. altitude dependence which can be represented both in the form of zonal models [5] and in the form of its measured values. The results of lidar thermal sounding from the Earth's surface can be used as an example [6].

Note that the strongest effect of the temperature profile variations on the quality of the results of microwave observations will be manifested during the so-called sudden stratospheric warming (SSW) events, where an increase in temperature by tens of degrees occurs at altitudes of 20–60 km.

Therefore, during these events, when measuring (estimating) the quantitative composition of the atmosphere, it is important to record its temperature profile. Warmings, as a rule, are accompanied by the

* yuyukul@appl.sci-nnov.ru

[1] Institute of Applied Physics of the Russian Academy of Sciences, Nizhny Novgorod; [2] V. E. Zuev Institute of Atmospheric Optics of the Siberian Branch of the Russian Academy of Sciences, Tomsk; [3] Higher School for Economics, Nizhny Novgorod, Russia. Translated from Izvestiya Vysshikh Uchebnykh Zavedenii, Radiofizika, Vol. 64, No. 12, pp. 927–941, December 2021. Russian DOI: 10.52452/00213462_2021_64_12_927 Original article submitted May 31, 2021; accepted December 28, 2022.

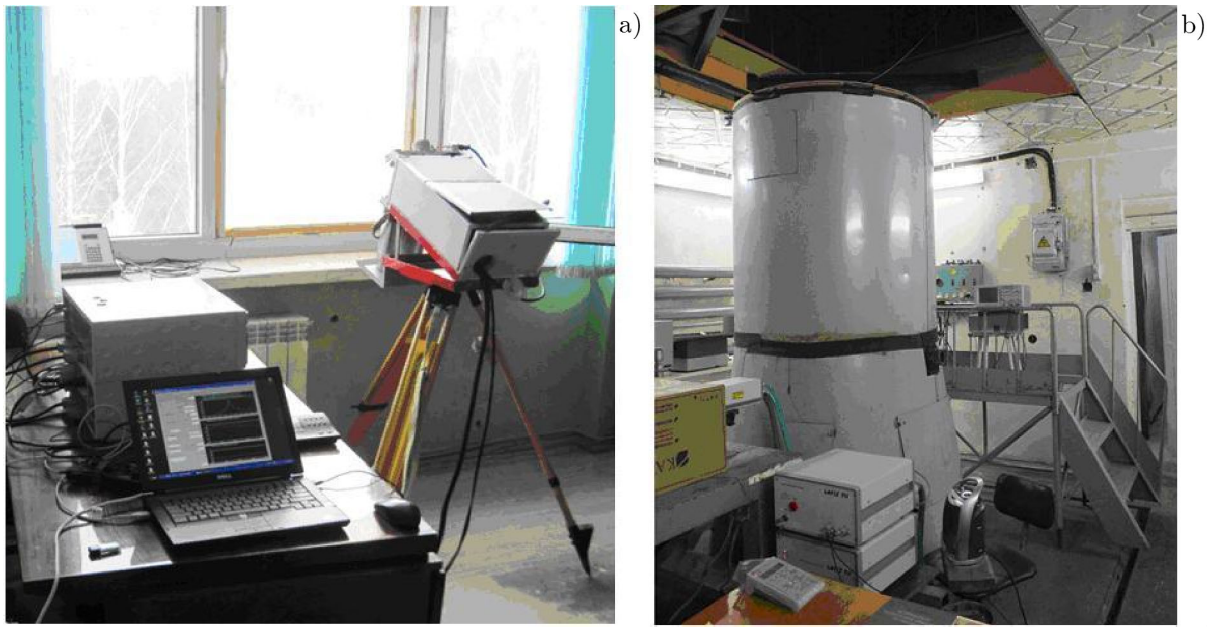

Fig. 1. General view of the measuring systems: mobile microwave ozonometer (a) and Rayleigh lidar (b).

destruction of the polar stratospheric cyclone. It is known that an extensive circumpolar vortex of cyclonic type is formed in the high-latitude stratosphere during winter. The high wave activity characteristic of the atmosphere of the Northern hemisphere during winter often leads to the deformation and destruction of the vortex. Although the winter atmosphere of Western Siberia is more stable compared to the European territory, the consequences of the destruction of the polar stratospheric cyclone and the perturbation of the stratospheric temperature mode are also manifested here.

The goal of this work is to carry out simultaneous measurements of ozone and temperature in the middle atmosphere using microwave and lidar technologies to diagnose the processes of atmospheric circulation restructuring with high spatiotemporal resolution.

This paper is dedicated to the memory of A. G. Kislyakov, a pioneer of research of the Earth's ozone layer at millimeter radio waves. The paper is the generalization of a series of works on the study of the middle atmosphere simultaneously in the microwave and optical wavelength ranges. This approach has been quite fruitful and gave an impetus to solving new problems in atmosphere physics. Note that intense studies on the interaction of the middle (altitudes of 20–100 km) and upper (altitudes of more than 100 km) atmosphere have been carried out in the last decade. This is evident from the publication activity of researchers from a number of countries [7–15].

2. MEASURING SYSTEMS

The most advanced and promising methods, including microwave radiometry and lidar diagnostics, were used in a joint experiment to study the middle atmosphere. A general view of the measuring systems employed in this experiment is shown in Fig. 1.

2.1. Mobile Microwave Ozonometer

The method of microwave ground-based radiometry is based on measurements of the rotational emission spectra of gas minorities (in our case, ozone) in the millimeter and submillimeter wavelength ranges. The results of microwave observations depend only weakly on weather conditions and the presence of aerosols in the atmosphere, which is an advantage compared to observations in the optical and infrared wavelength ranges. In addition, microwave ozone observations can be performed around the clock. In recent years, it has

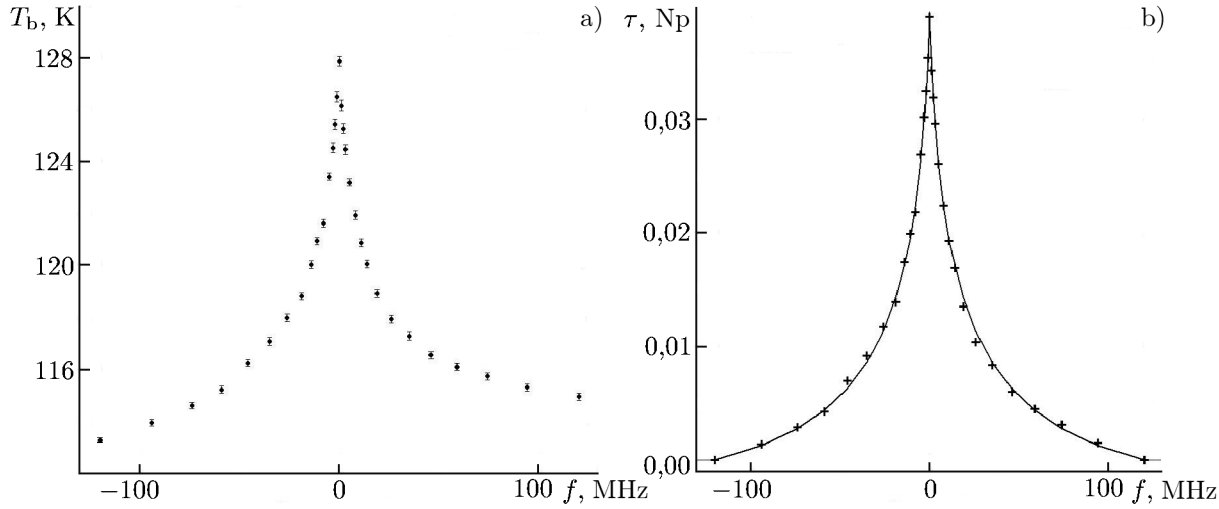

Fig. 2. Panel *a*: the radiation spectrum of the entire atmosphere in the ozone resonance line 110836.04 MHz measured at the antenna of the microwave spectrometer (T_b is the brightness temperature). Panel *b*: the modified spectrum of the ozone line for estimating the vertical profile of ozone (τ is the optical depth. The crosses correspond to experimental data and the solid line, to the spectrum calculated from the retrieved vertical profile of ozone). Tomsk, 02:17−02:37 LT on November 23, 2011.

been possible to make a significant step towards the creation of mobile microwave spectrometers of a new generation [16, 17]. The use of mobile ozonometers enabled one to perform in difficult expedition conditions a number of tasks, the solution of which would be difficult when a standard microwave technology is employed. Note that a completely new approach has been applied to microwave observations of ozone [18]. The essence of this approach is that observations use a rotational transition of O_3 at a frequency of 11.072 GHz. The shape of this atmospheric line in the entire neutral atmosphere at up to 100 km is determined only by the Lorentz broadening, and this makes it possible to correctly estimate the vertical profile of the O_3 concentration in the middle atmosphere.

Information about the O_3 concentration is contained in the measured spectrum of the integral radio emission of the middle atmosphere. Using the inversion of the obtained spectra, it is possible to find data on the vertical distribution of ozone in the atmosphere. For this purpose, a method of selecting the parameters of the vertical ozone distribution model [19] was employed. The method consisted in minimizing the r. m. s. differences of the measured spectra and the spectra calculated from the retrieved ozone profiles. In solving the problem of estimating the vertical profile of ozone, model dependences of pressure and temperature on altitude were used [5]. The criterion for a correct solution of the inverse problem was the best matching between the ozone spectral line calculated from the retrieved O_3 profile and the original experimental spectrum. The uncertainties in estimating the ozone profile depend on various kinds of errors in radiometric measurements of the O_3 line spectra. The error in determining the vertical distribution of ozone by its measured spectra using the above-described tool does not exceed 20%. Using a real temperature distribution to estimate the ozone profile will reduce the error in determining the vertical distribution of ozone to 10% in the altitude range 20–40 km. Figure 2*a* shows an example of the atmospheric radiation spectrum in the vicinity of the rotational resonance of the ozone line 110836.04 MHz measured at the horn antenna input. This is the dependence of the brightness temperature of atmospheric radiation on the frequency with allowance for water vapor, oxygen, and ozone. Figure 2*b* shows the modified spectrum (water vapor and oxygen were removed) in the form of a frequency dependence of the optical depth, which is related only to ozone.

The IAP RAS has developed and manufactured a mobile microwave radiometer for a study of the ozone layer [16, 17]. This instrument is a multichannel spectroradiometer of the millimeter wavelength range, which is tuned to a fixed frequency corresponding to the resonant frequency 110836.04 MHz of the rotational transition of the ozone molecule. The analyzed frequency band is about 240 MHz and the spectral resolution

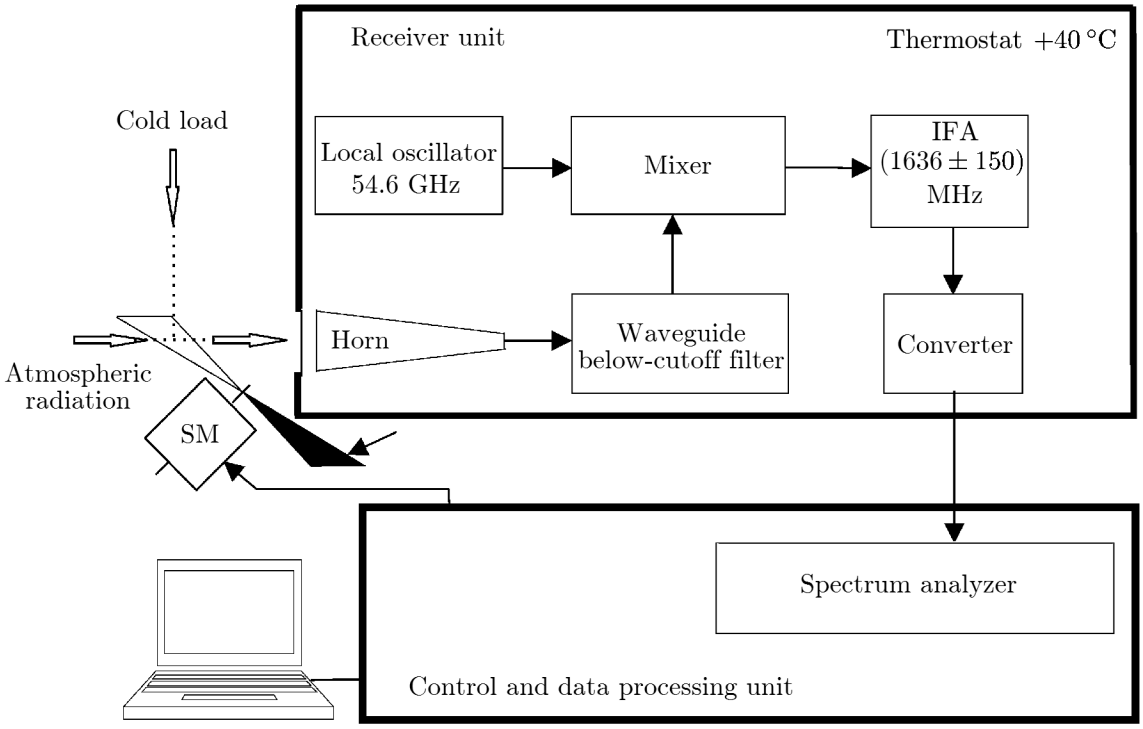

Fig. 3. Layout of a mobile microwave radiometer for a study of ozone in the middle atmosphere.

in the analysis of the ozone line center is 1 MHz. The noise temperature of the uncooled receiver in a single-band reception mode is 2500 K.

The layout of the instrument is shown in Fig. 3. In front of the horn there is a quasi-optical switch, i. e., a symmetrical flat impeller at the axis of the stepping motor (SM). One-half of the impeller is mirrored, and on the other, a microwave absorbing substance is pasted, which, in this case, is a warm calibration load for the receiver. This software-controlled switch provides that signals from the atmosphere and two calibration loads, namely, a warm load at the ambient temperature and a cold load at the boiling point of liquid nitrogen, are fed consistently to the receiver input. The radiation pattern at the receiver input is formed by a scalar horn and is approximately 5°. For the single-band mode of the receiver operation, a waveguide below-cutoff filter is used, suppressing the signal at the lower sideband frequency. The signal suppression coefficient of the mirror frequency is no less than 20 dB. Signal losses in the operating frequency band do not exceed 0.5 dB. The mixer is based on a Schottky barrier diode and operates at the second harmonic of the local oscillator. After the mixer, the signal enters the intermediate-frequency amplifier (IFA) and then passes through the intermediate frequency converter in the frequency range of the spectrum analyzer.

Figure 4 shows a general view of the input waveguide path unit. Due to the unit design, it was possible to minimize the spectrum distortions of the received signal that are caused by the interference of intrinsic input noise of the receiver.

3. Rayleigh Lidar

Lidar ground-based studies of the thermal state of the stratosphere and mesosphere above Tomsk started at the V. E. Zuev Institute of Atmospheric Optics SB RAS in 1994 [22]. Lidar measurements of the vertical temperature distribution are carried out by the method of elastic molecular (Rayleigh) and spontaneous combination (Raman) scattering of light and are based on an unambiguous relationship between the molecular backscattering coefficient and the atmospheric density at a certain altitude.

The lidar layout for measuring the vertical temperature distribution, as well as the vertical stratification of the aerosol, are shown in Fig. 5.

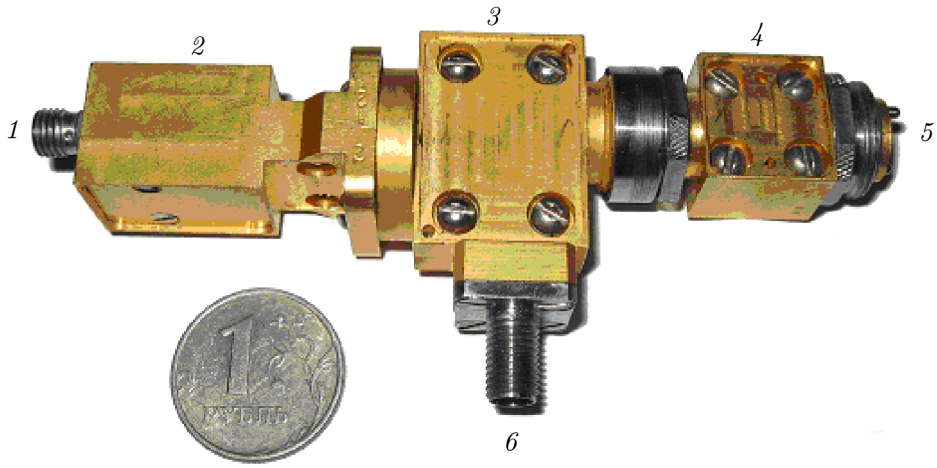

Fig. 4. General view of the input waveguide path unit: local oscillator at 18.2 GHz (*1*), multiplier by 3 (*2*), subharmonic mixer (*3*), mirror channel filter (*4*), 110.8 GHz input (*5*), intermediate frequency (1.6 GHz) output (*6*).

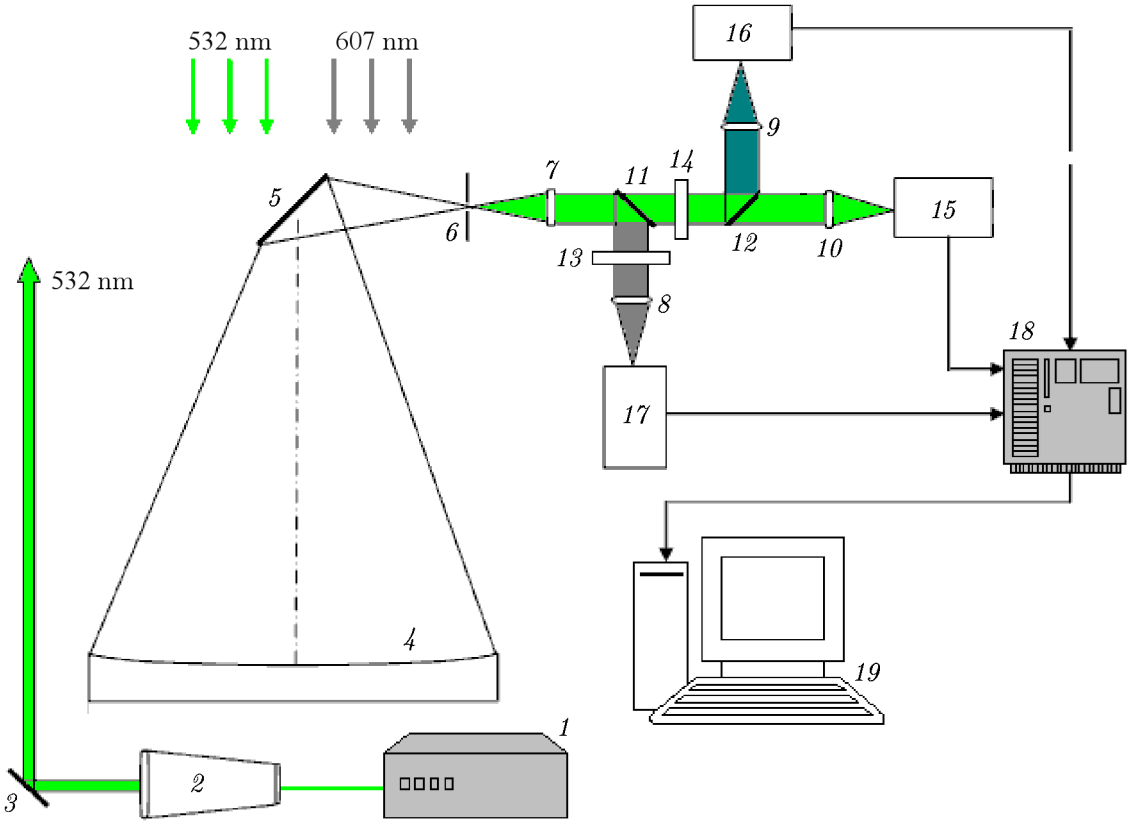

Fig. 5. Lidar layout: laser (*1*), collimator (*2*), flat mirror (*3*), main parabolic mirror (*4*), flat counter-reflector (*5*), diaphragm (*6*), focusing lenses (*7*, *8*, *9*, and *10*), dichroic plate (*11*), beam-splitting plate (*12*), interference light filters (*13* and *14*), photo sensor modules (*15*, *16*, and *17*), photon counter (*18*), and PC (*19*).

Lidar emitter *1* is an LS-2137U-UV3 laser, which is a special model of an AIG:Nd serial laser LS-2137U with electro-optical Q-factor modulation and conversion of the main generation wavelength (1.064 nm) into second-harmonic radiation (532 nm). The main technical parameters of the laser transmitter and receiving system are presented in Table 1. The laser beam is directed to the collimator *2*, and then the beam is vertically

TABLE 1. The main technical parameters of the laser.

Pulse energy, mJ	400
Pulse sending frequency, Hz	10
Pulse duration at a level of 0.5, ns	≤ 7
Laser beam diameter, mm	≤ 8
Energy fraction in the laser beam at a divergence level of 0.86 mrad	≤ 0.8
Polarization	linear
Beam divergence at the output, mrad	0.1

emitted into the atmosphere through a flat mirror *3*. The scattered radiation of the atmosphere enters the telescope of the Newton system *4* with a main-mirror diameter of 1 m and a focal length of 2 m. A field diaphragm *6*, designed to form the field of view of the receiving antenna and ultimately performing spatial signal selection, is installed in the telescope's focal plane. The optical signals filtered out from background noise are directed to the receiving unit, where their spectral selection and photoelectronic conversion are performed. This unit has four focusing lenses *7*, *8*, *9*, and *10*, a dichroic filter *11* for separating radiation at wavelengths of 532 and 607 nm, a plate *12* for separating radiation at a wavelength of 532 nm for beams with an approximate percentage relation of 10% and 90% (reduction of the dynamic range when receiving signals of the near and far zones), and interference light filters for wavelengths of 532 and 607 nm (*13* and *14*, respectively). Separated optical signals along three separate channels are transmitted through focusing lenses to sensor modules *15*, *16*, and *17*, where they are converted into electrical signals. This transformation is performed in the photon counting mode. Then the photons are recorded by photon counter *18* with further data transfer to PC *19* for collection and accumulation.

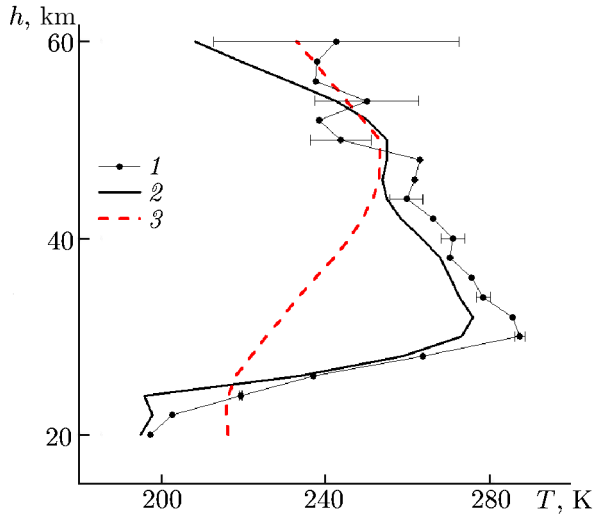

Fig. 6. Vertical temperature profile measured at the lidar station Tomsk IAO SB RAS at 19:44–21:18 LT on January 1, 2013 during extraordinary sudden stratospheric warming. The circles represent lidar data, the solid line, a temperature profile according to MLS/AURA satellite data, and the red dashed line, a temperature profile according to CIRA 86 model.

The lidar uses Hamamatsu H2859-01, PMT R7207-01, and H7422P-40 photo detectors with high spectral sensitivity and operation speed. Backscattering is received in the photon counting mode. Single-electron pulses are recorded by a photon counter, which has been developed at the Institute of Atmospheric Optics SB RAS. The facility is designed to receive signals from a photoelectronic multiplier to a PC. The sounding is carried out at night. The vertical resolution used for measuring the signal (strobe length) is 192 m. A single series of measurements was performed for 10 min, and the average measurement time per night was about two hours. Figure 6 shows an example of measuring the temperature profile in the atmosphere above Tomsk using the lidar. The measurement was performed on January 1, 2013.

The measurement error depends on the number of photons received from a given altitude. The number of photons is determined by the energy of the laser pulse, the duration of the strobe, the number of laser shots, the aerosol concentration, air density, and background noise. The errors indicated in Fig. 6 at altitudes of 20 to 40 km range from 1 to 3 K. In this case, the uncertainty in temperature measurement increases with altitude, and it increases to ± 10 K as the level 60 km is approached.

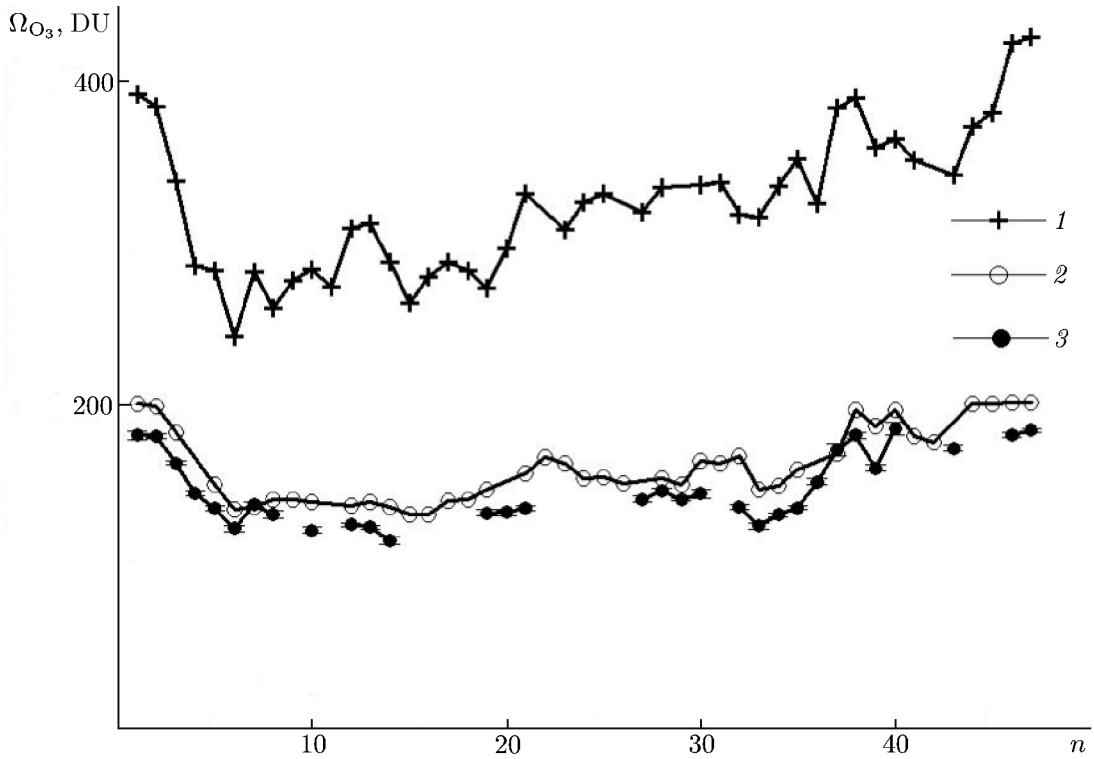

Fig. 7. Temporal variations in ozone content Ω_{O_3} during stratospheric warming in the winter of 2012–2013 above Tomsk, Western Siberia. Curve *1* represents the total ozone content according to OMI/AURA data, curve *2*, ozone content in the 20–50 km layer according to MLS/AURA data, and curve *3*, ozone content above 22 km according to the ground-based microwave measurements. Here, n is the number of the day starting from December 14, 2012.

4. THE RESULTS OF OBSERVATIONS AND THEIR ANALYSIS

4.1. The winter of 2012–2013

Microwave and optical observations of ozone and temperature were performed between December 14, 2012 and January 29, 2013. This period was chosen due to the fact that according to several years of lidar sounding above Tomsk (56° N, 85° E), stratospheric warmings, as a rule, occur in December–January. When analyzing the results of joint observations, aerological sounding data obtained at the Kolpashevo (58° N, 83° E) and Novosibirsk (55° N, 83° E) stations, which are located at about 250 and 210 km from Tomsk, respectively, were used. In addition, observation data from the AURA OMI/AURA (total ozone) and MLS/AURA (ozone and temperature) satellite instruments were employed. Ground-based microwave measurements typically lasted several hours before and after the sunset. After the sunset, the lidar was used to measure the temperature profiles [23, 24].

Figure 7 shows ozone content variations during the measurement campaign, namely the data from satellite-borne instruments on the total ozone content (OMI/AURA), ozone content in the 20–50 km layer (MLS/AURA), and the results of ground-based microwave sounding. All instruments detected a decrease by about 50% in the amount of ozone for a few days, starting from December 14, 2012. After December 20, a monotonic increase in ozone content was observed, which by January 29 had recovered to its original values.

Figure 8 shows ozone and temperature variations at the chosen altitudes 25 and 60 km in the middle atmosphere. The time dependence of the amount of ozone (filled circles) obtained from ground-based microwave measurements is also given. These data are the result of solving the problem of retrieval of the vertical profile of ozone using model dependences of pressure and temperature on altitude. The diamonds mark the microwave sounding data adjusted taking into account real temperature profiles measured by the

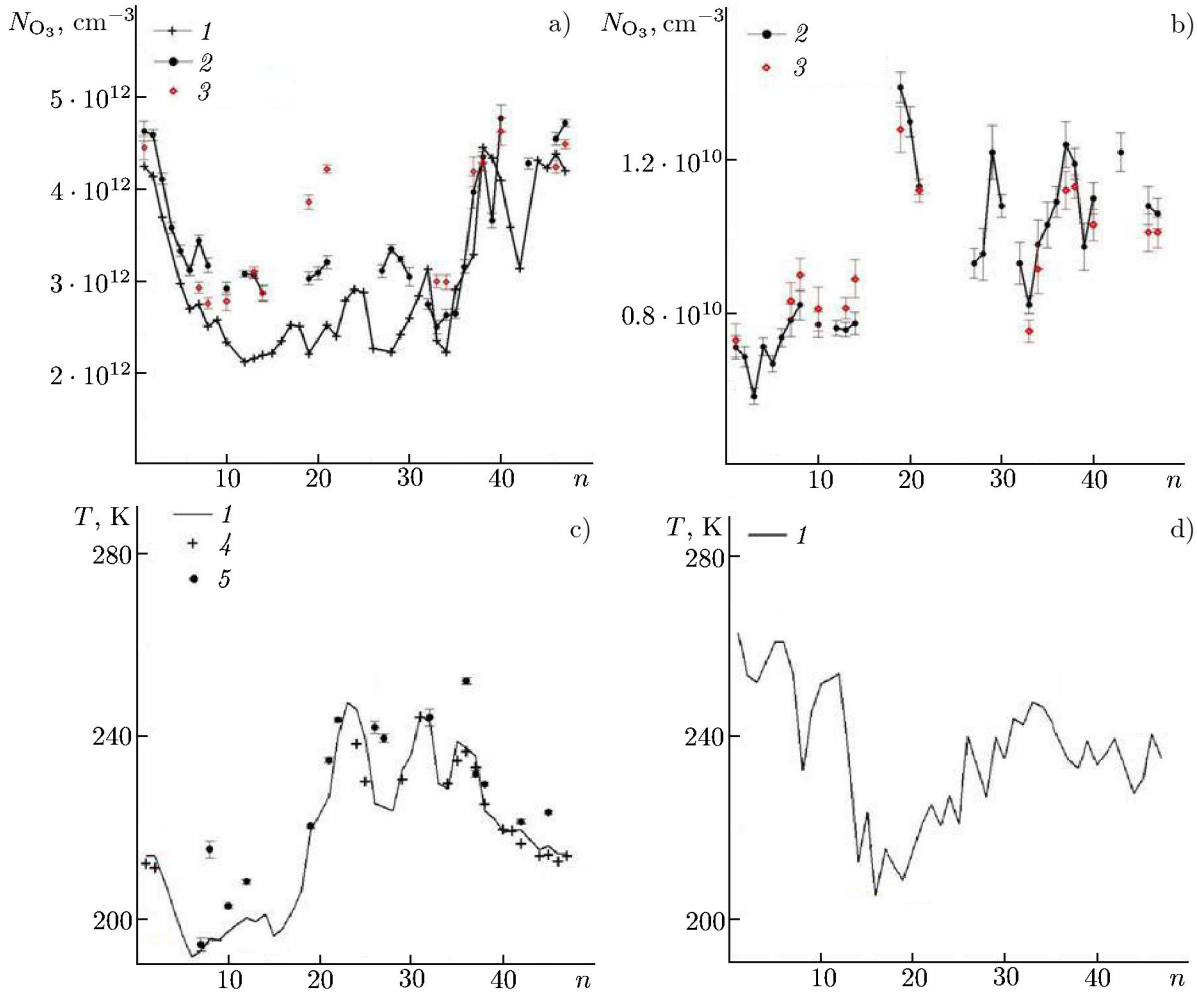

Fig. 8. Ozone and temperature variations above Tomsk at altitude of 25 km (*a*, *c*) and 60 km (*b*, *d*) during stratospheric warming in the winter of 2012–2013. Curves *1* correspond to the MLS/AURA data, curves *2*, to the microwave measurements, curves *3*, to the microwave measurements adjusted for the lidar-measured temperature profile, curve *4*, to the aerosol measurements, and curve *5*, to the lidar measurements. Here, n is the number of the day starting from December 14, 2012.

lidar and MLS/AURA. Crosses and the solid line indicate the MLS/AURA data.

Stratospheric warming, during which lidar and microwave measurements were carried out, was of the major type. As a result, a restructuring of the circulation in the stratosphere above Western Siberia from westward to eastward transfer took place. During the winter anomalous events, notable ozone and temperature variations in the middle atmosphere were detected. Ozone variations at altitude levels of 25 to 60 km ranged from 150% to 200%, while the amplitude of their oscillations significantly increased. The peak of the positive temperature deviation from the monthly average reached 70 K at an altitude of 30 km. Ozone diurnal variations at an altitude of 60 km related to sunset and sunrise were about 30%.

A feature of the observed stratospheric warming was the effect of a significant time delay in the growth of ozone content at altitudes of 20–30 km in relation to the temperature increase by about 20 days, which was detected by both ground-based and orbital tools.

In the range of altitudes 40–60 km, the correlation between ozone and temperature variations was negative. The correlation value varied from -0.59 to -0.45 depending on the altitude. Apparently, the behavior of ozone in the middle atmosphere at all altitudes was greatly determined by the dynamic processes caused by the destruction of the high-altitude polar vortex.

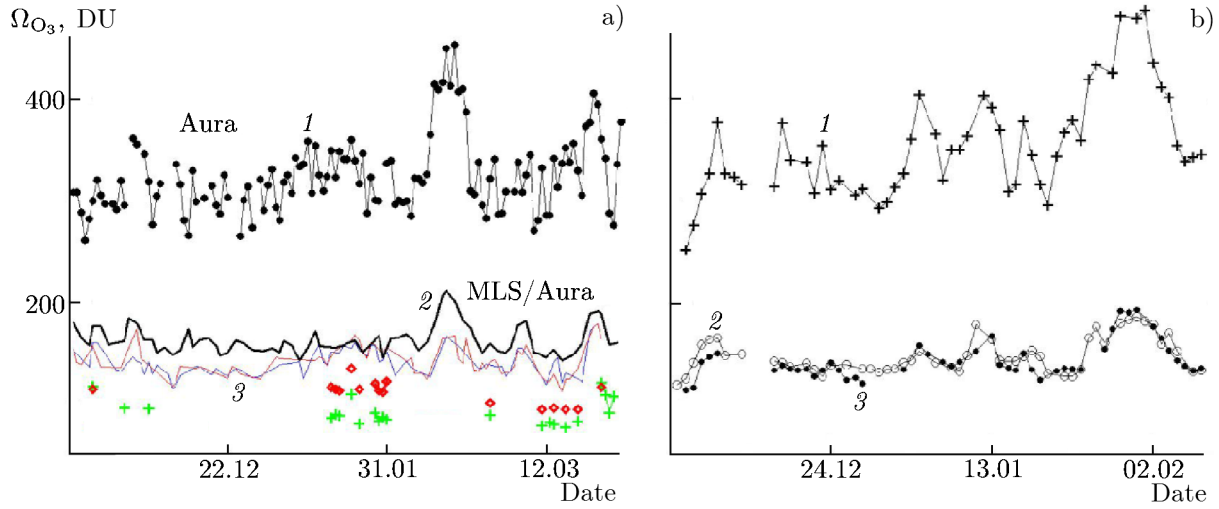

Fig. 9. Atmospheric ozone content variations in the winter of 2013–2014 above Peterhof (a) and Tomsk (b). Curves *1* correspond to the total ozone content according to OMI/AURA data, curves *2*, to the ozone content in the 20–50 km layer according to MLS/AURA data, and curves *3*, to an ozone content higher than 22 km according to microwave measurements, while on panel a, the red thin line corresponds to daytime data and the blue one, to the night-time data. Ground-based measurements of the integral ozone content above 25 km are also presented on panel a, namely, microwave sounding data (red diamonds) and infrared observations of the Bruker IFS-125HR Fourier spectrometer (green crosses).

4.2. The winter of 2013–2014

Below we present the results of simultaneous ozone measurements in the middle atmosphere in Peterhof (60° N, 30° E) and Tomsk (56° N, 85° E) during stratospheric warming in the winter of 2013–2014. Identical microwave ozonometers were employed in the experiment. It is very important to use here the same methods of both observations and estimates of the vertical distribution of ozone in the middle atmosphere. The results of ground-based microwave measurements were compared with microwave data on the altitude profiles of ozone and temperature in the layer above 22 km (MLS/AURA), as well as with satellite-borne data (OMI/AURA) on the total ozone content. The data of microwave measurements of the ozone content in the 25–60 km layer were compared with the results obtained using the Bruker IFS-125HR infrared Fourier spectrometer in Peterhof [27].

Figure 9 shows ozone content variations in November—March of 2013–2014 above Peterhof (a, c) and in December—February of 2013–2014 above Tomsk (b, d).

We now consider the ozone behavior in this season in the Peterhof area (Figs. 8a and 8c). Perturbations in the ozone content above 22 km, which started in mid-February and lasted till the end of March, are clearly seen. The first maximum of ozone content (microwave data) appeared on February 15, 2013, the second maximum corresponded to March 7, 2014, and the third one, to March 25, 2014. The alternation of maxima occurred with a time interval of about 20 days. In this case, the ozone variations determined by satellite-borne and ground-based microwave measurements are identical.

We now address Fig. 10 showing the time course of ozone (ground-based microwave sounding data) and temperature (MLS/AURA data) at altitudes of 25, 40, and 60 km above Peterhof and Tomsk in the winter of 2013–2014. According to these data, the stratospheric warming that developed above Peterhof followed the conventional top-down scheme. This was supported by the ozone and temperature variations at an altitude of 40 km, shifted in time relative to the data at an altitude of 25 km. The increase in temperature and ozone at an altitude of 40 km was approximately two weeks ahead of the temperature and ozone variations at an altitude of 25 km. Microwave observations we performed earlier in polar latitudes have repeatedly confirmed such a scenario of the ozone evolution during stratospheric warming [4]. We note a significant ozone-content

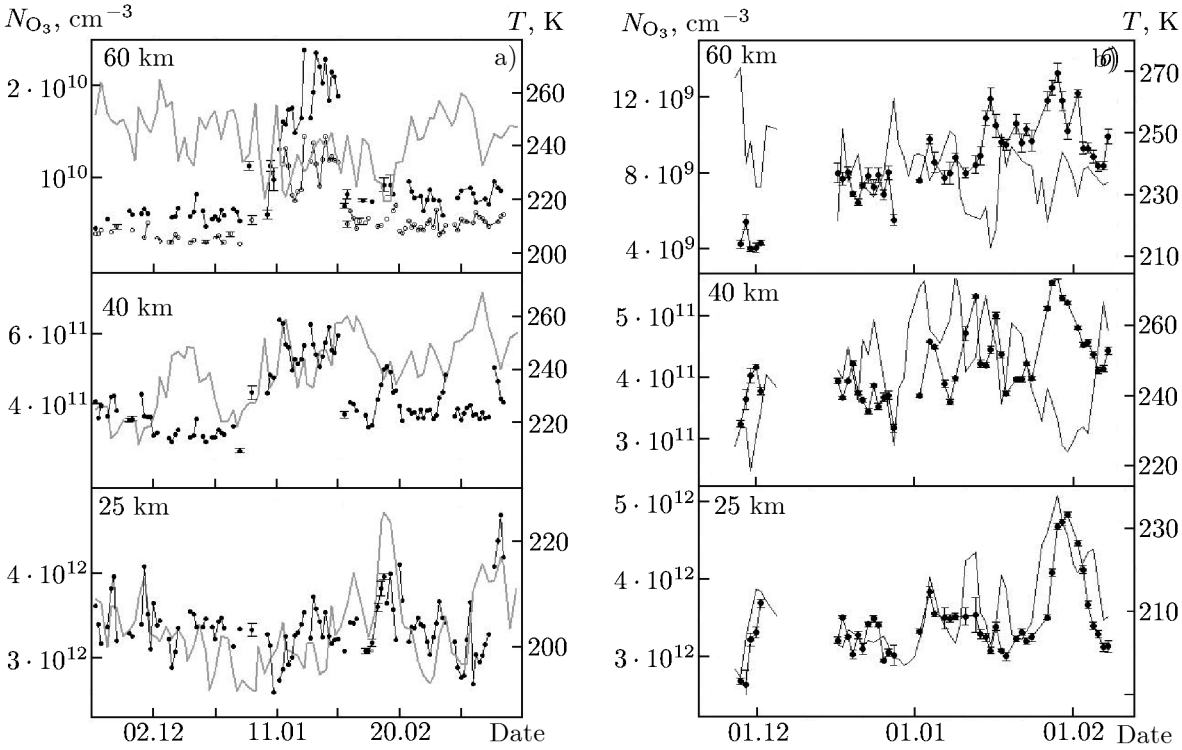

Fig. 10. Ozone and temperature variations in the middle atmosphere in the winter of 2013–2014 above Peterhof (a) and Tomsk (b) for altitudes of 25, 40, and 60 km. Solid curves correspond to temperature measurements using the MLS/AURA satellite-borne instrument and the curves with markers, to ozone concentration according to ground-based microwave sounding. On panel a, for an altitude of 60 km, filled circles correspond to nighttime data and empty circles, to daytime data.

perturbation at altitudes of 40 and 60 km in the second half of January 2014. The amount of ozone at an altitude of 40 km increased with respect to the unperturbed interval by about 70%, and the increase reached several hundred percent at a level of 60 km [26]. Discrepancies between satellite-borne and ground-based data, except for the second half of January, stayed within a 10% accuracy of microwave radiometry. During the development of warming in the middle and upper stratosphere, the satellite did not detect perturbations in the ozone layer, unlike the data obtained from the Earth's surface. Microwave observations of ozone and temperature variations in the middle atmosphere in the winter of 2013–2014 in Peterhof (60° N, 30° E) and in Tomsk (56° N, 85° E) showed a difference in the behavior of the above parameters. It should be noted that Peterhof is much closer to the center of the winter polar vortex than Tomsk.

A dynamic process of stratospheric warming was recorded above Peterhof in the altitude range 22–60 km from mid-January to almost the end of March 2014. The warming developed from top to bottom, and the largest ozone variations (a few hundred percent) took place at altitudes of 40–60 km. At altitudes below 40 km, the ozone variations were 20–50%. The time interval between ozone variations in the upper and lower stratosphere was about two weeks.

In the winter of 2013–2014, the vertical structure of the ozone layer was also formed above Tomsk due to dynamic processes, but to a large extent these changes were caused not so much by the stratospheric warming as by the powerful eastward transfer of air masses at altitudes of 20–40 km.

4.3. The winter of 2014–2015

Ground-based microwave observations were performed from December 5, 2014 to February 9, 2015. In this time period, the number of lidar sounding sessions was small, and the vertical temperature profiles

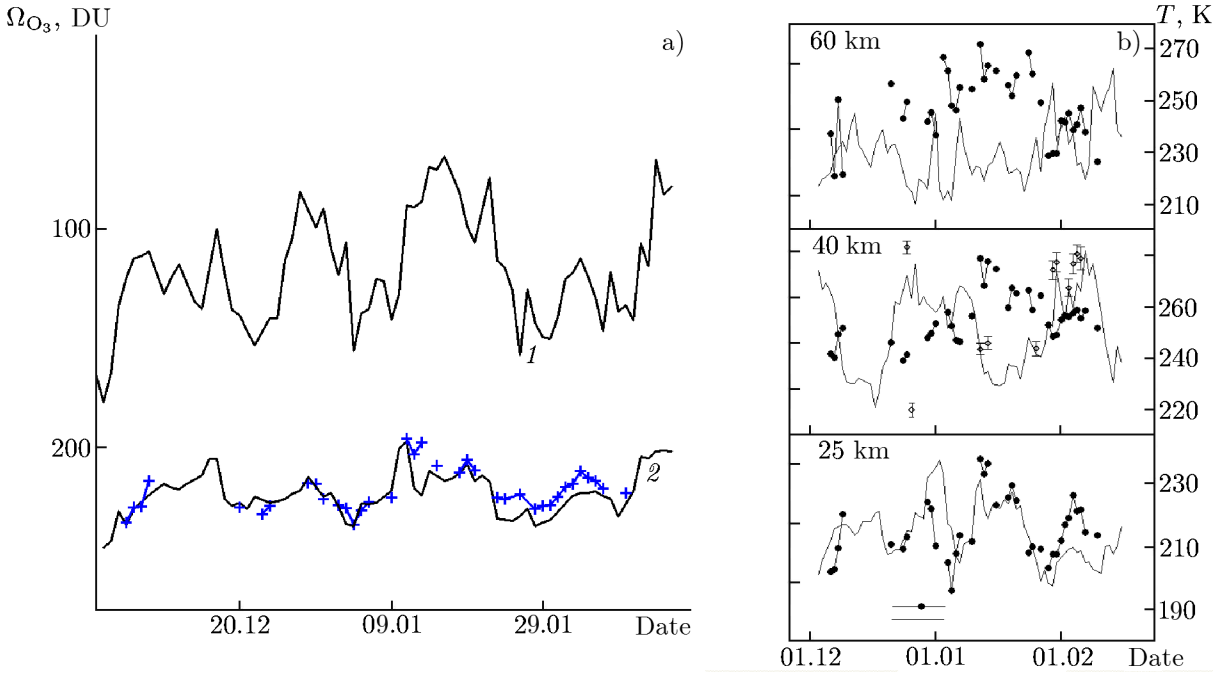

Fig. 11. Panel *a*: variations in the total ozone content (curve *1* according to OMI/AURA data), in the ozone content in the 20–50 km layer (according to MLS/AURA data, curve *2*) and in the ozone content in the layer above 22 km (according to microwave sounding, blue crosses). Panel *b*: variations in ozone (filled circles) and temperature (solid line, according to MLS/AURA data) for altitudes of 25, 40, and 60 km. For an altitude of 40 km, the temperature values measured by the lidar (empty diamonds) are also given.

were reliable at altitudes of 30 to 60 km. Stratospheric warming in the winter of 2014–2015 had a long duration. According to lidar observations, the start of the warming was detected on November 11, 2014. The warming reached its greatest development on November 27, when it covered an altitude range of 30 to 55 km with a maximum positive temperature deviation from the monthly average to up 60 K at an altitude of 35 km. This effect was also observed with a slightly smaller increase in temperature in the MLS/AURA satellite-borne observations. In December, another stratospheric perturbation followed, which was detected in both lidar and satellite-borne observations. This stratospheric warming was observed between December 3 and December 24 in the same altitude range 30–55 km. The next wave of warming was detected at the end of January 2015, and it lasted till the end of the second decade of February. It should be emphasized that this was one of the longest stratospheric warmings recorded in lidar observations above Tomsk since 1996. The greatest positive temperature deviations were observed on February 5 in the altitude range 40–45 km and reached 60 K at an altitude of 40 km.

Figure 11 shows ozone-content variations based on the results of ground-based microwave measurements and satellite-borne measurements using OMI/AURA and MLS/AURA, as well as variations in O_3 concentration and temperature at selected altitudes of 25, 40, and 60 km above Tomsk in the winter of 2014–2015.

A feature of the winter of 2014–2015 was quasi-periodic variations in ozone content and temperature, which were observed at an altitude of 40 km. There was a correlation between ozone and temperature variations at an altitude of 25 km.

5. CONCLUSIONS

The conducted series of microwave and optical observations of ozone and temperature in the middle atmosphere in Western Siberia during a sudden stratospheric warming yielded a number of new results.

A detailed picture of ozone and temperature variations above Tomsk during warming of both major

and minor types has been constructed.

Significant ozone variations from 150% to 200% at altitudes of 25 to 60 km during major warming in the winter of 2012–2013 were recorded. Ozone variations at an altitude of 60 km with a duration of about 30 days, which occurred during the restructuring of the air mass circulation in the upper stratosphere from western to eastern transfer, were detected.

Microwave observations of the middle atmosphere in the winter of 2013–2014 in Peterhof and Tomsk showed a significant difference in the behavior of ozone and temperature.

In the winter of 2014–2015, lidar temperature measurements detected the longest stratospheric warming in Tomsk since 1996: it lasted almost a month.

The paper shows that the combination of ground-based microwave and lidar observations is optimal for research and monitoring of ozone fields and temperature in the middle atmosphere.

This work was performed within the framework of the State assignment for the IAP RAS (project No. 0030–2021–0008) and was supported by the Russian Foundation for Basic Research (project Nos. 18–45–520009 and 19–45–703034).

REFERENCES

1. M. R. Schoeberl, *Rev. Geophys.*, **16**, No. 4, 521–538 (1978). https://doi.org/10.1029/RG016i004p00521
2. G. L. Manney, M. J. Schwartz, K. Krüger, et al., *Geophys. Res. Lett.*, **36**, No. 12, L12815 (2009). https://doi.org/10.1029/2009GL038586
3. J. W. Waters, L. Froidevaux, R. S. Harwood, et al., *IEEE Trans. Geosci. Remote Sens.*, **44**, No. 5, 1075–1092 (2006). https://doi.org/10.1109/TGRS.2006.873771
4. Y. Y. Kulikov, A. A. Krasil'nikov, and V. G. Ryskin, *Izv. Atmosph. Ocean Phys.*, **38**, No. 2, 158–166 (2002).
5. J. J. Barnett and M. Corney, in: K. Labitzke, J. J. Barnett, and B. Edwards, eds., *Handbook for MAP*, Vol. 16, SCOSTEP (1985), p.p. 47–85.
6. V. N. Marichev, *Opt. Atmosf. Okeana*, **24**, No. 5, 386–391 (2011).
7. L. P. Goncharenko, A. J. Coster, R. A. Plump, et al., *Geophys. Res. Lett.*, **39**, No. 8, L08101 (2012). https://doi.org/10.1029/2012GL051261
8. L. Goncharenko, J. L. Chau, P. Condor, et al., *Geophys. Res. Lett.*, **40**, No. 19, 4982–4986 (2013). https://doi.org/10.1002/grl.50980
9. M. A. Chernigovskaya, E. N. Sutyrina, and K. G. Ratovsky, *Sovr. Probl. Dist. Zond. Zeml. Kosm.*, **11**, No. 2, 264–274 (2014).
10. G. G. Matvienko, Y. Y. Kulikov, V. N. Marichev, et al., in: *ILRC 27 EPJ Web Conf., 2016*, **119**, 24002. https://doi.org/10.1051/epjconf/2016119224002
11. E. Turunen, A. Kero, P. T. Verronen, et al., *JGR Atmosph.*, **121**, No. 19, 11852–11861 (2016). https://doi.org/org/10.1002/2016jD025015
12. N. M. Pedatella, J. L. Chau, H. Schmidt, et al., *EOS*, **99**, No. 6, 35–38 (2018). https://doi.org/10.1029/2018EO092441
13. A. S. Yasyukevich, M. V. Klimenko, Y. Y. Kulikov, et al., *Solar-Terr. Phys.*, **4**, No. 4, 48–58 (2018). https://doi.org/10.12737/stp-44201807
14. Y. Y. Kulikov, A. V. Poberovskii, V. G. Pyskin, et al., *Geomagn. Aeron.*, **60**, No. 2, 254–262 (2020). https://doi.org/10.1134/S0016793220020097
15. N. V. Bachmetieva, Y. Y. Kulikov, and I. N. Zhemyakov, *Atmosphere*, **11**, No. 11, 1154–1175 (2020). https://doi.org/10.3390/atmos11111154

16. Y. Y. Kulikov, A. A. Krasil'nikov, and A. M. Shchitov, in: *Proc. Int. Kharkov Symp. Phys. Engineering Microwaves, Millimeter, Submillimeter Waves, Kharkov, Ukraine, June 25–30, 2007*, Vol. 1, pp. 62–66.

17. A. A. Krasil'nikov, Y. Y. Kulikov, V. G. Ryskin, et al., *Instrum. Exp. Tech.*, **54**, No. 1, 118–123 (2011). https://doi.org/10.1134/S0020441211010167

18. A. E. E. Rogers, M. Lekberg, and P. Pratar, *J. Atmosph. Oceanic Techn.*, **26**, No. 10, 2192–2199 (2009). https://doi.org/org/10.1175/2009jTECHA1291.1

19. J. De La Noë, A. Baudry, M. Perault, et al., *Planet. Space Sci.*, **16**, No. 7, 737–741 (1983). https://doi.org/10.1016/0032-0633(83)90122-8

20. Y. Y. Kulikov, N. N. Markina, A. P. Naumov, et al., *Izv. Akad. Nauk SSSR Fiz. Atmos. Okeana*, **24**, No. 12, 1282–1292 (1988).

21. Y. Y. Kulikov, I. V. Kuznetsov, A. F. Andriyanov, et al., *J. Geophys. Res.*, **99**, No. D10, 21109–21116 (1994). https://doi.org/10.1029/94JD01102

22. G. G. Matvienko, B. A. Banakh, S. M. Bobrovnikov, et al., *Opt. Atm. Okeana*, **22**, No. 10, 915–930 (2009).

23. V. N. Marichev, G. G. Matvienko, A. A. Lisenko, et al., *Atmos. Oceanic Opt.*, **26**, No. 3, 222–226 (2013).

24. Y. Y. Kulikov, A. A. Krasilnikov, V. G. Ryskin, et al., in: *Proc. Int. Kharkov Symp. Phys. Engineering Microwaves, Millimeter, and Submillimeter Waves, Kharkov, Ukraine, June 23–28, 2013*, Vol. 1, pp. 480–482. https://doi.org/10.1109/MSMW2013.6622106

25. V. N. Marichev, G. G. Matvienko, A. A. Lisenko, et al., *Atmos. Oceanic Opt.*, **27**, No. 6, 499-505 (2014).

26. D. A. Bochkovsky, Y. A. Virolainen, Y. Y. Kulikov, et al., *Radiophys. Quantum Electron.*, **59**, No. 4, 270–277 (2016). https://doi.org/10.1007/s11141-016-9702-x

27. Y. A. Virolainen, Y. M. Timofeev, A. V. Poberovsky, et al., *Izv. Atmos. Oceanic Phys.*, **51**, No. 2, 167–176 (2015). https://doi.org/10.1134/S0001433815020127